

Shape Control in Marangoni-Driven Patterning

Steven K. Stanley and Roger T. Bonnecaze

*Department of Chemical Engineering
University of Texas at Austin; Austin, TX 78712*

ISCST-20180918AM-B-MD4

Presented at the 19th International Coating Science and Technology Symposium,
September 16-19, 2018, Long Beach, CA, USA[†].

Introduction: Variations in liquid surface tension cause surface-shear driven flow, which is known as the Marangoni effect. The Marangoni effect has been harnessed to pattern thin polymer films by applying a photochemically induced surface energy or tension gradient to the films through the use of a UV light source and photomask [1–6]. By heating the film above its glass transition temperature, the polymer flows from the unexposed regions of lower surface tension into the patterned, higher surface tension regions, creating hill and valley features that resemble the initial photomask pattern. A schematic of the process is shown in Fig. 1.

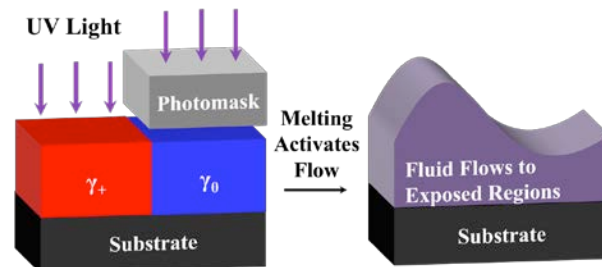


Figure 1. Schematic of Marangoni-driven patterning. Polystyrene film is exposed to UV light through a photomask. A small amount of the polystyrene is dehydrogenated making the surface tension or energy higher in the exposed region. Heating the film above its glass transition temperature allows the polymer to flow into and accumulate in the exposed, higher surface tension regions.

If the time when the polymer is mobile is prolonged, the surface tension promoter diffuses, thereby weakening the surface tension gradient and eventually capillary forces replanarize the film. However, if the film is quenched before significant diffusion has occurred, the hill and valley features can be locked into place. This process is called Marangoni-driven patterning and is similar to traditional photolithography. Marangoni-driven patterning possesses its own sets of advantages and disadvantages with respect to traditional photolithography. For instance, Marangoni-driven patterning can employ simpler polymers and does not require developing solvents, but rather relies on a simple heating step to activate the flow. On the other hand, Marangoni-driven patterning currently produces feature sizes with critical dimensions of 1-10 microns and aspect ratio features around 0.04 [6]. Traditional lithography is capable of generating features on the order tens of nanometers and aspect ratios well above unity. Despite this fact, Marangoni-driven patterning could lend itself to niche applications such as improving light capturing efficiency in photonic devices [7] and enhancing solar cell efficiency [8]. Furthermore, Marangoni-driven patterning could be adapted to roll-to-roll production methods and create cheaper pathways to these and other applications.

One barrier to advancing the state of the art in Marangoni-driven patterning is mask design. Most experiments have employed binary, contact photomasks that do not compensate for the pattern bias and corner rounding effects inherent to the flow process. Here, we present a method to optimize a photomask for Marangoni-driven patterning by applying techniques similar to optical proximity correction (OPC) used

[†] Unpublished. ISCST shall not be responsible for statements or opinions contained in papers or printed in its publications.

in photolithography (note that contact printing does not suffer from diffraction effects). We compensate for the flow effects by iteratively simulating the flow process, contouring and comparing the resulting pattern to the target, and biasing the photomask for ten iterations. We present the model used to simulate Marangoni-driven patterning and the algorithm used to adjust the photomask. We then present an optimized photomask to form a square pattern and show that the resulting pattern contour is significantly improved by adjusting the photomask.

Methodology: Arshad *et al.* developed a model and simulation tool for line-and-space Marangoni-driven patterning in their study of polystyrene and poly(phenyl acetylene) as the primary thin film components [9]. Upon exposure to UV light, some polystyrene subunits undergo a dehydrogenation reaction along the carbon-carbon backbone to produce a copolymer of polystyrene and poly(phenyl acetylene). The poly(phenyl acetylene) is known to impart a higher surface tension to the film relative to the polystyrene and is responsible for the Marangoni flow that results when the film is melted. To model the flow, Arshad *et al.* utilized the thin film equation,

$$\frac{\partial h}{\partial t} = \nabla \cdot \left\{ \left[\frac{h^2}{2\mu} \nabla \gamma \right] + \left[\frac{h^2}{3\mu} \nabla (\gamma \nabla^2 h) \right] \right\}, \quad (1)$$

to describe how the polymer-air interface evolved in time, along with the convection diffusion equation,

$$\frac{\partial C}{\partial t} = \nabla \cdot \left\{ D \nabla C - C \left[\frac{h^2}{\mu} \nabla \gamma + \frac{h^2}{2\mu} \nabla (\gamma \nabla^2 h) \right] \right\}, \quad (2)$$

to describe the transport of the surface tension promoter. ∇ is the two-dimensional gradient operator acting in the x - and y - directions, parallel to the surface. Here, h is the film height, t is time, μ is the polymer viscosity, γ is the surface tension, which is assumed to be a linearly related to the species concentration C , and D is the diffusion coefficient. The surface tension was calculated by using a linear mixing rule, weighting the pure polymer surface tension values by their respective mole fractions. Symmetry boundary conditions in h and C were implemented effectively simulating a periodic system in the x - and y - directions. Arshad *et al.* implemented the model using parameters that were estimated at temperatures used in accompanying experiments and the parameters are summarized in ref. [9]. Simulations showed good quantitative agreement with the experiments. We have implemented this same model and physical parameters at 140 °C in the study here. The initial film height h_0 and pitch w were 150 nm and 105 microns, respectively. The initial conversion, C_0 , of polystyrene to poly(phenyl acetylene) was 0.064 (and is also the mole fraction poly(phenyl acetylene)). These and other physical parameters are shown in Table 1.

Table 1: Physical parameters used in simulation.

Parameter	h_0 (nm)	w (μm)	γ (mN/m) Polystyrene	γ (mN/m) Poly(phenyl acetylene)	μ (Pa-s)	D (10^{-14} m ² /s)	C_0 (mole frac.)
Value	150	105	30.8	34.0	154	5.91	0.064

The model was solved using a fourth-order accurate finite difference algorithm. The domain was a 105x105 micron square and was discretized into a 109x109 point domain with $\Delta x = \Delta y = 0.97$ microns. An adaptive time-stepping algorithm was implemented to maximize the time step while still maintaining accuracy. The initial photomask pattern was a 35x35 micron dark field square. Because contact printing does not suffer greatly from diffraction effects, we assumed ideal image transfer. The normalized concentration of poly(phenyl acetylene) over the domain was initialized by setting all points that fell within or on the square to unity and those points that fell without the square to 0.01. Fig. 2 shows the initial concentration pattern and the evolution of the film at various times. Initially, the Marangoni forces cause the polymer to flow into the exposed square. Initially, four peaks form that flow towards the center where the surface tension is greatest and they eventually merge around $t = 8$ minutes. After reaching a peak structure around $t = 37$ minutes, the pattern dies away due to diffusion of the surface tension promoter and capillary forces.

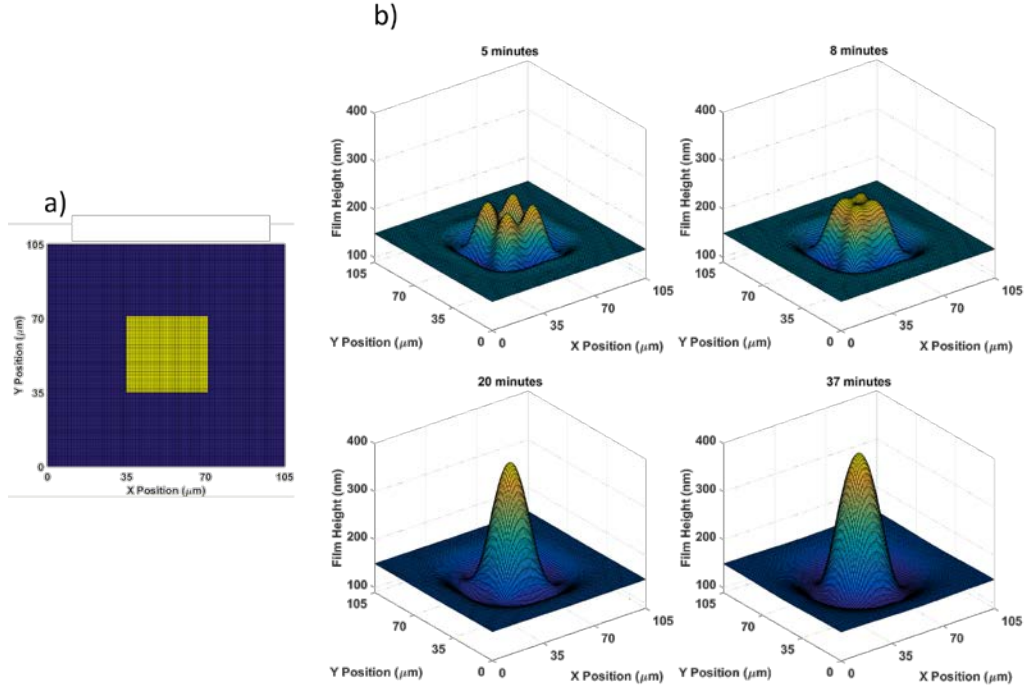


Figure 2. a) Initial concentration profile, where yellow regions possess a higher concentration of surface tension promoter and blue squares possess a lower concentration. b) Feature progression over time.

Notice that at the nominal film height (150 nm), the feature contour initially resembles that of the desired square shape (the initial photomask) and degrades to a circle at longer times. To achieve both the desired square shape and taller features, an algorithm was developed to iteratively bias the photomask and compensate for the feature shrinkage. The objective of the algorithm was to minimize the average edge displacement between the pattern contour, \mathbf{P} , and the target 35x35 micron square contour, \mathbf{T} . \mathbf{P} and \mathbf{T} were a collection of M and N points, respectively, which were extracted using contour functions available in MATLAB. The edge displacement error at a given point on the pattern contour was defined as

$$EDE_i = \min(\|\mathbf{P}_i - \mathbf{T}_j\|) \quad \text{for } j = 1, 2, \dots, N, \quad (2)$$

where EDE_i is the edge displacement error at point i , \mathbf{P}_i is the pattern contour position at index i , and \mathbf{T}_j is the target contour position at index j . The average edge displacement error was defined as

$$AEDE = \frac{1}{M} \sum_{i=1}^M EDE_i \quad \text{for } i = 1, 2, \dots, M, \quad (2)$$

where $AEDE$ is the average edge displacement error, which served as the objective function to be minimized. Fig. 3 shows how the average edge displacement error changes over time for the simulation shown previously in Fig. 2. Fig. 3 also shows how the feature height evolves over time. Here feature height is defined as the height above the nominal film height measured at the center of the feature.

Fig. 3 shows that the average edge displacement error increases until roughly 20 minutes, after which it begins to decrease. More importantly, the feature height at early times is negative (indicating that fluid is drawn away from the center). A negative feature height is undesirable because the feature would provide no etch resistance in those regions. To avoid the issue of negative feature height, early times were avoided for the optimizations presented here.

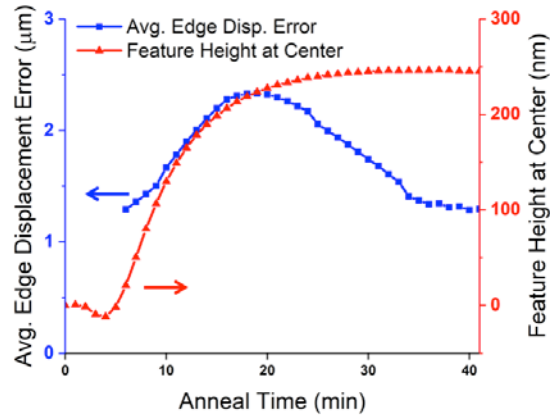


Figure 3. Average edge displacement error and feature height at center for simulation shown in Fig. 2. Left axis corresponds to *AEDE*. *AEDE* is not shown for early times due to contouring issues. Right axis corresponds to the feature height at center.

To modify the mask for optimization purposes, a polygon-manipulation scheme was developed. The mask pattern was modified by expanding or shrinking the pattern in the horizontal direction by a single pixel as shown in Fig. 4, where the exposed regions are shown in yellow and the unexposed regions are shown in blue. The mask was kept symmetric by manipulating one-eighth of the pattern and mirroring the changes in the other seven sections. Note that if a pixel defining the edge of the pattern fell beyond the diagonal, that pixel was turned off (assigned a concentration of 0.01).

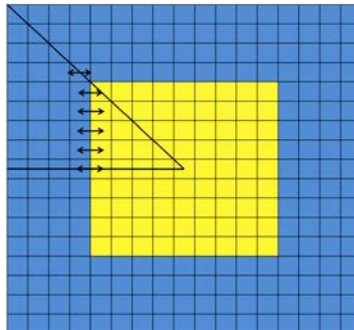


Figure 4. Cartoon illustrating how the photomask pattern was manipulated. Exposed regions are shown in yellow and unexposed regions are shown in blue. Edge pixels were grown and shrunk by a single pixel as shown by the double-headed arrows. Pixels that fell beyond the diagonal were turned off. Note that the pattern was manipulated only near the pattern boundary, as shown by the termination of the arrows around the square corner. Only one-eighth of the pattern was manipulated as shown by the triangular region. This region was then mirrored into the other seven regions.

To optimize the photomask, the fluid flow simulation was run to determine the *AEDE* at the nominal mask condition. Each edge pixel was then independently grown and shrunk and the simulation was run again to determine the *AEDE* at the modified conditions. The condition with the best *AEDE* (edge growth, shrinkage, or nominal condition) was applied to the next photomask iteration. Note that to avoid excessive island formation (isolated exposed pixels), only those pixels adjacent to the pattern boundary were modified. This is shown in Fig. 4 where the arrows terminate near the square corner. Rather than set tolerance-based criteria for termination, the iteration process was simply carried out ten times. Over the iteration process, the simulation time was fixed to 425, 500, 650, and 800 seconds. As stated previously, the lower bound of 425 seconds was chosen to avoid negative feature heights.

Results and Discussion: Fig. 5a shows the best *AEDE* seen across the ten iterations. The corresponding feature height is also shown. Note that the 800-second fixed simulation time showed the lowest *AEDE* and largest feature height and was therefore chosen for further analysis. Fig. 5b shows the

AEDE and feature height over all iterations for the fixed simulation time of 800 seconds and shows that the *AEDE* is reduced from 2 microns down to about 0.25 microns over ten iterations. This eight-fold improvement in *AEDE* is encouraging as it shows the feature contour can be greatly improved by applying iterative optimization techniques. The initial iterations show a dramatic improvement in average edge displacement error accompanied by a slight worsening of the feature height.

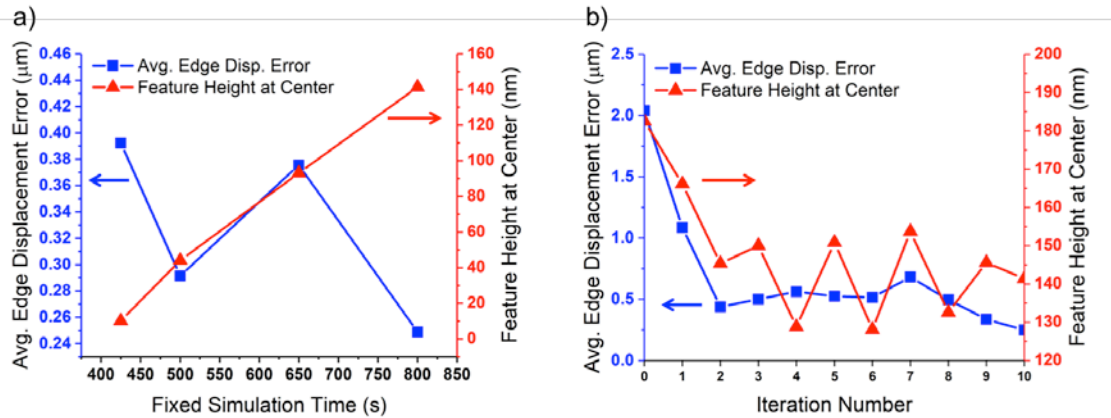


Figure 5. a) Comparison of the best *AEDE* seen across the ten iterations for fixed simulation times of 425, 500, 650 and 800 seconds. Feature height at the corresponding iteration is also shown. b) Comparison of average edge displacement error and feature height at different iterations for a fixed simulation time of 800 seconds.

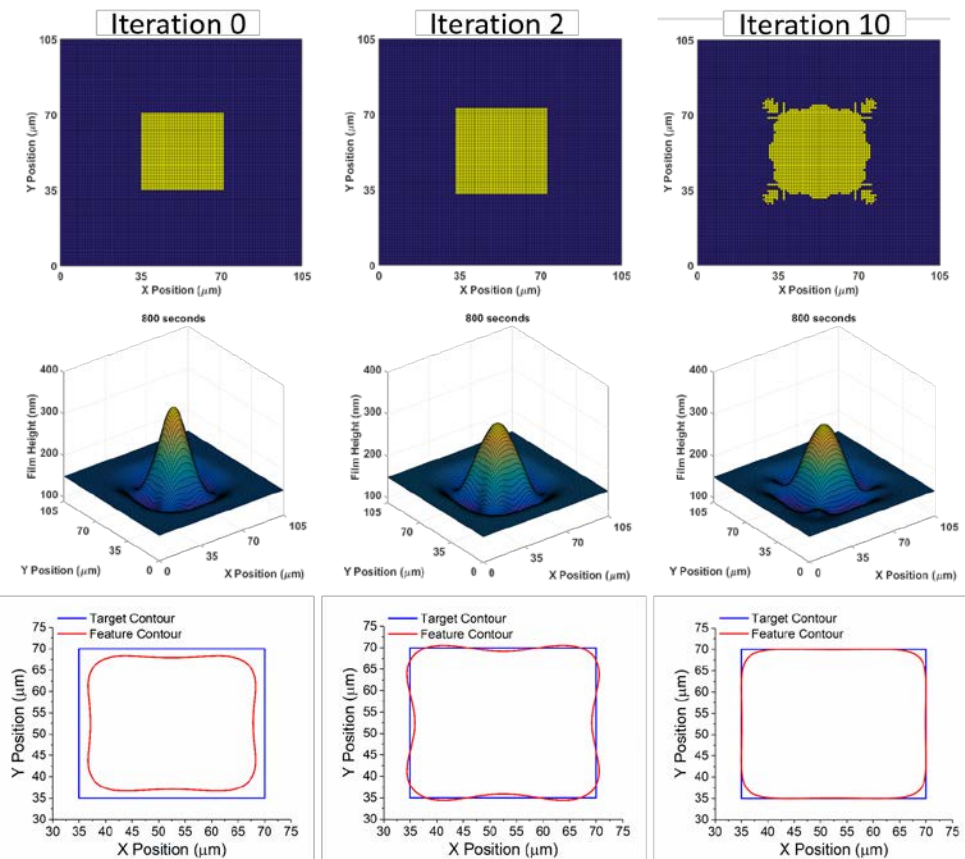


Figure 6. Photomask patterns, resulting contours vs. the target pattern, and feature surface plots at select iterations.

To better explain the results of Fig. 5b, Fig. 6 presents the actual photomask patterns, contours, and feature surface plots at select iterations. It can be seen that the first iterations add a simple outward bias to the mask while later iterations grow the corners of the mask and add complexity to continue improving the average edge displacement error. Note that the corners still exhibit significant rounding. Future work will be dedicated to minimizing corner rounding.

Conclusions: Here Marangoni-driven patterning was modeled for an initial square photomask pattern which resulted in a feature contour with significant *AEDE*. The large *AEDE* was mitigated by rationally adjusting the photomask through an optimization scheme. Ten iterations were performed for various fixed simulation times and the 800-second fixed simulation time was chosen for further study due to its improved *AEDE* and feature height. The tenth photomask iterate for the 800-second fixed time showed an eight-fold reduction in *AEDE* compared to the initial photomask. These results demonstrate through simulation that feature contours produced through Marangoni-driven patterning can be greatly improved by applying iterative optimization techniques.

Future work will include modifying the optimization scheme to account for corner rounding. We look forward to verifying the effectiveness of the optimization technique through experiments where a contact photomask will be taped out and used to print actual features.

References

- [1] J.M. Katzenstein, D.W. Janes, J.D. Cushen, N.B. Hira, D.L. McGuffin, N.A. Prisco, C.J. Ellison, Patterning by photochemically directing the Marangoni Effect, *ACS Macro Lett.* 1 (2012) 1150–1154. doi:10.1021/mz300400p.
- [2] D.W. Janes, J.M. Katzenstein, K. Shanmuganathan, C.J. Ellison, Directing convection to pattern thin polymer films, *J. Polym. Sci. Part B Polym. Phys.* 51 (2013) 535–545. doi:10.1002/polb.23262.
- [3] C.J. Bin Kim, C., Janes, D. W., McGuffin, D. L., & Ellison, Surface energy gradient driven convection for generating nanoscale and microscale patterned polymer films using photosensitizers, *J. Polym. Sci. Part B Polym. Phys.* 52 (2014) 1195–1202.
- [4] J.M. Katzenstein, C. Bin Kim, N.A. Prisco, R. Katsumata, Z. Li, D.W. Janes, G. Blachut, C.J. Ellison, A photochemical approach to directing flow and stabilizing topography in polymer films, *Macromolecules.* 47 (2014) 6804–6812. doi:10.1021/ma5010698.
- [5] C. Bin Kim, D.W. Janes, S.X. Zhou, A.R. Dulaney, C.J. Ellison, Bidirectional Control of Flow in Thin Polymer Films by Photochemically Manipulating Surface Tension, *Chem. Mater.* 27 (2015) 4538–4545. doi:10.1021/acs.chemmater.5b01744.
- [6] A.R. Jones, C.B. Kim, S.X. Zhou, H. Ha, R. Katsumata, G. Blachut, R.T. Bonnecaze, C.J. Ellison, Generating large thermally stable Marangoni-driven topography in polymer films by stabilizing the surface energy gradient, *Macromolecules.* 50 (2017) 4588–4596.
- [7] H. Koo, W. H., Jeong, S. M., Araoka, F., Ishikawa, K., Nishimura, S., Toyooka, T., Takezoe, Light extraction from organic light-emitting diodes enhanced by spontaneously formed buckles, *Nat. Photonics.* 4 (2010) 222–226.
- [8] J.B. Kim, P. Kim, N.C. Pégard, S.J. Oh, C.R. Kagan, J.W. Fleischer, H. a. Stone, Y.-L. Loo, Wrinkles and deep folds as photonic structures in photovoltaics, *Nat. Photonics.* 6 (2012) 327–332. doi:10.1038/nphoton.2012.70.
- [9] T.A. Arshad, C.B. Kim, N.A. Prisco, J.M. Katzenstein, D.W. Janes, R.T. Bonnecaze, C.J. Ellison, Precision Marangoni-driven patterning., *Soft Matter.* 10 (2014) 8043–50. doi:10.1039/c4sm01284d.